Theoretical physics.
Theory of condensed matter

UDC 538.9

EDN ZLXASG
https://www.doi.org/10.33910/2687-153X-2023-4-4-176-194

Calculations of Lyapunov exponents and characterizations of nonlinear dynamics in bulk antiferroelectrics

S.-Ch. Lim✉[1]

[1] Universiti Sains Malaysia, 11800 USM Penang, Malaysia

Author

Siew-Choo Lim, ORCID: 0000-0001-8397-0886, e-mail: sclim@usm.my

For citation: Lim, S.-Ch. (2023) Calculations of Lyapunov exponents and characterizations of nonlinear dynamics in bulk antiferroelectrics. *Physics of Complex Systems*, 4 (4), 176–194. https://www.doi.org/10.33910/2687-153X-2023-4-4-176-194 EDN ZLXASG

Received 15 July 2023; reviewed 21 September 2023; accepted 21 September 2023.

Funding: The study did not receive any external funding.

Abstract. This paper investigates the influence of the amplitude, frequency, and damping of the applied field on the maximal Lyapunov exponents and chaotic dynamics in the bulk antiferroelectric (AFE) system. Numerical simulations are conducted in three parts. First, Wolf's algorithm calculates the Lyapunov exponents with varying frequencies and a constant amplitude. The second part varies the amplitude while keeping the frequency constant. Two sets of data are generated for small ($g = 0.01$) and large ($g = 0.3$) damping values. In the third part, selected parameters produce phase portraits based on the positive and negative Lyapunov exponents using the fourth-order Runge–Kutta method. The results show that the Lyapunov exponent identifies chaotic and periodic regimes with small damping, but this becomes less evident with large damping. The study also demonstrates that manipulating the applied field parameters enables control over chaotic and periodic responses in the bulk AFE system.

Keywords: Lyapunov exponents, antiferroelectrics, ammonium dihydrogen phosphate, chaos, nonlinear, periodic response

Introduction

There are various methods to characterize the nonlinear and chaotic dynamics of physical systems. For example, one method involves plotting the power spectrum versus finite applied frequencies, where the nonlinear properties are revealed through the structures, positions, and intensities of the spectrum peaks (Dykman et al. 1988). The other methods include plotting phase portraits, Poincaré sections, and calculating the Lyapunov exponents (Baker, Gollub 1996; Goldstein et al. 2002; Marion, Thornton 1995; Strogatz 2015). In the phase portraits method, the shape of the curves and their overlap indicates the periodic responses of dynamical systems to external driving forces. Poincaré sections, on the other hand, are periodic snapshots of phase portraits, providing further insight into the behavior of nonlinear systems through the distributions and overlap of points in the 2D plots generated by these sections. The Lyapunov exponents method involves calculating the rate of exponential divergence of neighboring phase trajectories. The Lyapunov exponents greater or less than zero serve as hallmarks of chaotic or periodic responses, respectively, of the system states with respect to driving forces. Among these methods, the Lyapunov exponent is an important indicator for understanding the chaotic dynamics of physical systems. By combining these methods, a clearer picture of the dynamical responses of the system can be obtained. In this paper, we adopt a combination of methods by calculating the Lyapunov exponent and utilizing phase portraits to analyze selected parameters.

There are numerous methods available to determine the Lyapunov exponents. Some of these methods include the fast Lyapunov indicator, which computes the average of the largest Lyapunov exponent obtained from orthonormal basis tangent vectors in the phase space of the dynamical system (Lega et al. 2016). Ulam's method is used to calculate the maximal Lyapunov exponent for one-dimensional systems under small perturbations (Benettin et al. 2018). Another method involves calculating the finite size Lyapunov exponent based on averaging the finite amplitude growth rate of the dynamical physical system (Meunier, LaCasce 2021). Wolf's algorithm is employed to estimate the Lyapunov exponents for analytically defined time series model systems (Wolf et al. 1985). In this paper, we adopt Wolf's algorithm to calculate the Lyapunov exponents of bulk antiferroelectrics (AFE) (Wolf et al. 1985).

The research presented in this paper is an extension of (Lim 2022), focusing on investigating the effects of frequency, amplitude of the driving field, and damping in antiferroelectrics on the maximal Lyapunov exponents and nonlinear chaotic dynamics observed in the bulk antiferroelectric (AFE) system during its first ordered phase. The numerical simulations conducted in this study are divided into three parts. In the first two parts, Wolf's algorithm is utilized to calculate the Lyapunov exponents of the bulk AFE system. The first part involves varying the frequency of the applied field while keeping the amplitude constant. The second part focuses on varying the amplitude of the applied field while keeping the frequency constant. For each set of the selected amplitude and frequency of the applied field, two sets of numerical data are generated to account for different damping conditions. Specifically, one set corresponds to a small damping value of $g = 0.01$, and the other set corresponds to a large damping value of $g = 0.3$.

In the third part, a few sets of parameters are selected from the first two parts, corresponding to positive and negative values of the Lyapunov exponents, which are then used to generate the corresponding phase portraits. The method employed in the third part closely resembles that of (Lim 2022), where numerical simulations are conducted using the fourth-order Runge-Kutta method for a specific material, such as ammonium dihydrogen phosphate (ADP). In contrast to the approach in (Lim 2022), where the chaotic dynamics are explored through the generation of numerous phase portraits, we utilize the Lyapunov exponent as an indicator to distinguish between chaotic (positive) and periodic (negative) regimes.

Formalism for nonlinear dynamics

The details of the formalism can be found in (Lim 2022). The focus of the studies here is an extension of (Lim 2022), where we adopt Lim's dimensionless AFE oscillatory equations of motion, as shown in equations (1):

$$\frac{d^2q}{dt^2} + g\frac{dq}{dt} = -2(\psi+\tau)q + 4\left(q^3 + 3qr^2\right) - 6\left(q^5 + 10q^3r^2 + 5qr^4\right) + e_0\sin(2\pi ft), \tag{1a}$$

$$\frac{d^2r}{dt^2} + g\frac{dr}{dt} = -2\tau r + 4\left(3q^2r + r^3\right) - 6\left(5q^4r + 10q^2r^3 + r^5\right). \tag{1b}$$

The symbols τ, e ($\equiv e_0\sin(2\pi ft)$), q, r, ψ, t, and g represent the reduced or dimensionless temperature, applied Maxwell field, normal displacement, staggered displacement, interaction constant of sublattices, time, and damping, respectively. From equations (1), we choose e and g as the control parameters of the system for numerical simulations. In this paper, we fix the values of τ to be approximately -3.346457×10^{-3} and ψ to be approximately 1.2332677×10^{-2} as in (Lim 2022). The selected damping constants are 0.01 and 0.3.

Equations (1) are nonautonomous differential equations due to the explicit time dependence. In order to perform numerical simulations using Wolf's algorithm, these equations are transformed into autonomous differential equations (Baker, Gollub 1996; Boyce, DiPrima 2001) by introducing the following substitutions:

$$x_1 = q, \quad x_2 = r, \quad x_3 = 2\pi ft, \quad x_4 = \frac{dx_1}{dt} = \frac{dq}{dt}, \quad x_5 = \frac{dx_2}{dt} = \frac{dr}{dt}, \tag{2a}$$

$$x_6 = \frac{dx_3}{dt} = 2\pi f.$$

This yields six coupled first-order differential equations:

$$\frac{dx_1}{dt} = \frac{dq}{dt} = x_4, \tag{2b}$$

$$\frac{dx_2}{dt} = \frac{dr}{dt} = x_5, \tag{2c}$$

$$\frac{dx_3}{dt} = x_6 = 2\pi f, \tag{2d}$$

$$\begin{aligned}\frac{dx_4}{dt} &= -gx_4 - 2(\psi + \tau)x_1 + 4\left(x_1^3 + 3x_1x_2^2\right) \\ &\quad - 6\left(x_1^5 + 10x_1^3x_2^2 + 5x_1x_2^4\right) + e_0 \sin(x_3),\end{aligned} \tag{2e}$$

$$\begin{aligned}\frac{dx_5}{dt} &= -gx_5 - 2\tau x_2 + 4\left(3x_1^2x_2 + x_2^3\right) \\ &\quad - 6\left(5x_1^4x_2 + 10x_1^2x_2^3 + x_2^5\right),\end{aligned} \tag{2f}$$

$$\frac{dx_6}{dt} = 0. \tag{2g}$$

Numerical simulations

In the numerical simulations, we adopt the AFE's natural frequency, f_0, to be approximately 0.021336524, and the coercive field of the system, e_C, to be approximately 0.41658, as stated in (Lim 2022). The numerical simulations are divided into three parts. The first part is the Lyapunov exponents, λ_q, versus the frequency, f, of the applied field. The second part is the Lyapunov exponents, λ_q, versus the amplitude of the applied field, e_0. In the third part, we investigate the relations between the Lyapunov exponents and the AFE order parameter responses based on a few selected sets of parameters. The selections of these parameters are mainly based on the results obtained in the first and second parts. To eliminate transient effects, the first 30 cycles are excluded when generating the numerical data. The Lyapunov exponents in the first and second parts are obtained from the 31st to the 200th cycles.

Lyapunov exponents versus frequency of the applied field

The first part involves calculating the Lyapunov exponents, λ_q, of the AFE by varying the frequency f, while keeping the amplitude, e_0, and damping constant, g, fixed at certain values. Wolf's algorithm is utilized to compute the four Lyapunov exponents for q, dq/dt, r, and dr/dt, corresponding to x_1, x_4, x_2, and x_5 in equations (2). Only the largest Lyapunov exponents, λ_q, corresponding to q or x_1 are plotted in 2D graphs. In the calculations, for each selected fixed e_0 value, two curves are generated: one with a small damping constant, g = 0.01, and another with a large damping constant, g = 0.3. The numerical curves for λ_q versus f, with e_0 fixed at $0.01e_C$ and $0.9e_C$, are plotted in Figure 1, while the curves e_0 fixed at $2.0e_C$ are plotted in Figure 2. Furthermore, the curves with e_0 fixed at $249e_C$ are plotted in Figure 3. In Figures 1 and 2, the frequency, f, varies from $0.025\,f_0$ to $10.0\,f_0$, while in Figure 3, the frequency, f, varies from $0.25\,f_0$ to $100.0\,f_0$.

 https://www.doi.org/10.33910/2687-153X-2023-4-4-176-194

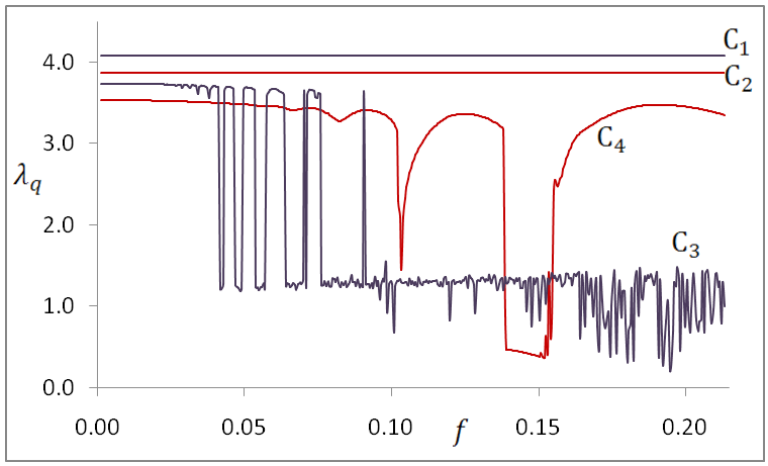

Fig. 1. λ_q versus f for $e_0 < e_C$. C_1 ($e_0 = 0.01e_C$, $g = 0.01$), C_2 ($e_0 = 0.01e_C$, $g = 0.3$); C_3 ($e_0 = 0.9e_C$, $g = 0.01$), C_4 ($e_0 = 0.9e_C$, $g = 0.3$)

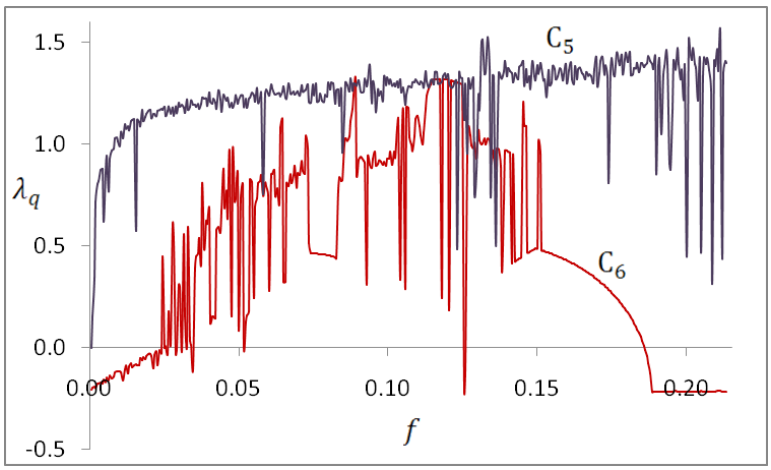

Fig. 2. λ_q versus frequency f for $e_0 > e_C$. C_5 ($e_0 = 2.0e_C$, $g = 0.01$), C_6 ($e_0 = 2.0e_C$, $g = 0.3$)

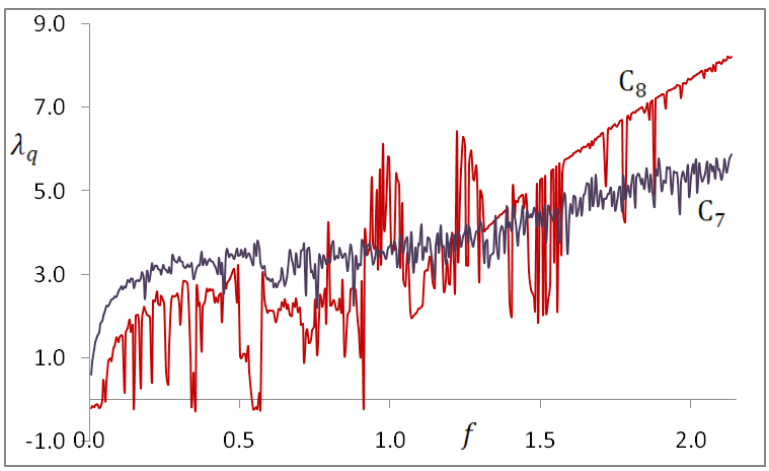

Fig. 3. λ_q versus f for $e_0 = 249e_C$. C_7 ($g = 0.01$), C_8 ($g = 0.3$)

The Lyapunov exponents, λ_q, versus frequency f with the amplitude fixed at $e_0 = 0.01e_C$, are represented by curves C_1 for $g = 0.01$ and C_2 for $g = 0.3$, as shown in Figure 1. The frequency, f, varies from $0.025\,f_0$ to $10.0\,f_0$. The curves C_1 and C_2 remain relatively at around 4.074 and 3.87, respectively, as the frequency varies. However, the numerical data for C_1 and C_2 exhibit slight fluctuations within the ranges [4.073846, 4.074086] and [3.870382, 3.870610], respectively. These small fluctuations disappear when C_1 and C_2 are plotted in the same graph. Generally, C_1 is approximately 0.204 higher than C_2.

The Lyapunov exponents, λ_q, versus frequency, f, with the amplitude fixed at $e_0 = 0.9e_C$, are represented by curves C_3 for $g = 0.01$ and C_4 for $g = 0.3$, as shown in Figure 1. In the frequency range $f \in [0.025f_0, 1.925f_0]$, curve C_3 is greater than C_4, and both curves have small fluctuations. For frequencies in the range $f \in [1.925f_0, 3.55f_0]$, curve C_3 demonstrates larger fluctuations within the range [3.6960336,1.2019837]. For frequencies greater than $3.55f_0$, curve C_4 exceeds C_3, except for the range $f \in [6.5f_0, 7.25f_0]$.

The Lyapunov exponents, λ_q, versus frequency f with the amplitude fixed at $e_0 = 2.0e_C$, are represented by curves C_5 for $g = 0.01$ and C_6 for $g = 0.3$, as shown in Figure 2. The frequency, f, varies from $0.025\,f_0$ to $10.0\,f_0$. In general, curve C_5 is greater than C_6, and both curves exhibit fluctuations throughout the entire range of the graph, i. e., $f \in [0.025f_0, 10.0f_0]$. For curve C_5, the first data point of λ_q is negative at $f = 0.025f_0$, while the remaining points are positive. Curve C_6, on the other hand, exhibits periodic windows, with notable ones occurring at $f \in [0.025f_0, 1.125f_0]$, $f \in [5.875f_0, 5.9f_0]$, and $f \in [8.725f_0, 10.0f_0]$.

The Lyapunov exponents, λ_q, versus frequency, f, with amplitude fixed at a large value, i. e., $e_0 = 249.0e_C$, are represented by curves C_7 for $g = 0.01$ and C_8 for $g = 0.3$, as shown in Figure 3. The frequency, f, varies from $0.25\,f_0$ to $100.0\,f_0$. In general, curve C_7 is higher than C_8 within the range $f \in [0.25f_0, 43.5f_0]$. Curve C_8 exhibits prominent fluctuation features in the range $f \in [43.5f_0, 7.375f_0]$. For frequencies greater than $7.375f_0$, curve C_8 tends to be higher than C_7, and demonstrates a trend of linear increment with respect to e_0. Curve C_7 does not exhibit periodic windows, while curve C_8 exhibits periodic windows.

By comparing curves C_1 to C_8 in Figures 1 to 3, we observe that the Lyapunov exponents, λ_q, for $g = 0.01$ are generally greater than those for $g = 0.3$, particularly for small e_0 and f values. Most of the periodic windows, where $\lambda_q < 0$, are present in the curves associated with the larger damping constant, $g = 0.3$, namely C_6 and C_8.

Lyapunov exponents versus amplitude of the applied field

In the second part, we use the same Wolf's algorithm as in the first part to compute the Lyapunov exponents for the AFE system by varying the amplitude of the applied field, e_0, while keeping its frequency, f, fixed at several values. The calculated values of λ_q are shown in Figures 4 and 5. For each selected fixed f value, two curves are generated: one with a small damping constant, $g = 0.01$, and another one with a large damping constant, $g = 0.3$.

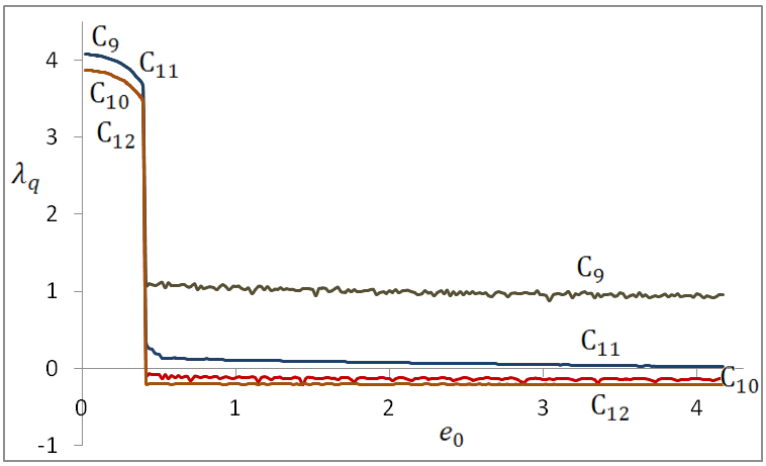

Fig. 4. λ_q versus e_0 for $f < f_0$. C_9 ($f = 0.5f_0$, $g = 0.01$), C_{10} ($f = 0.5f_0$, $g = 0.3$), C_{11} ($f = 0.04f_0$, $g = 0.01$), C_{12} ($f = 0.04f_0$, $g = 0.3$)

 https://www.doi.org/10.33910/2687-153X-2023-4-4-176-194

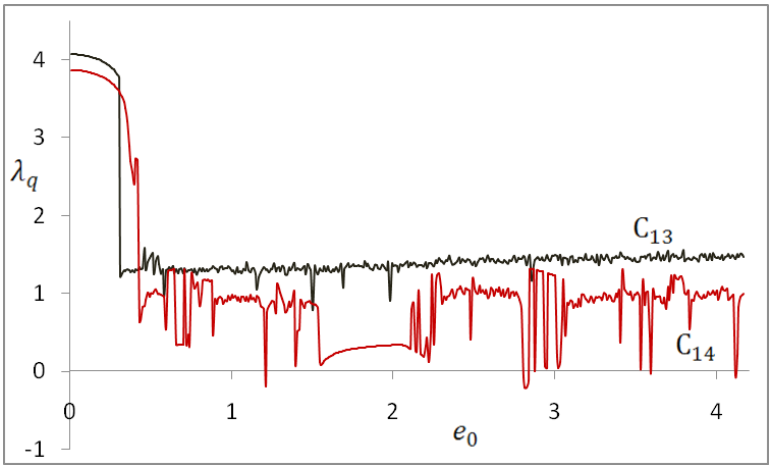

Fig. 5. λ_q versus e_0 for $f > f_0$. C_{13} ($f = 5.0\,f_0$, $g = 0.01$), C_{14} ($f = 5.0\,f_0$, $g = 0.3$)

The Lyapunov exponents, λ_q, versus amplitude, e_0, with the frequency fixed at $f = 0.5\,f_0$, are represented by curves C_9 for $g = 0.01$ and C_{10} for $g = 0.3$ in Figure 4. Additionally, the λ_q values with the frequency fixed at $f = 0.04f_0$ are represented by curves C_{11} for $g = 0.01$ and C_{12} for $g = 0.3$, as shown in Figure 4. The amplitude, e_0, varies from $0.025e_C$ to $10.0e_C$. In Figure 4, all curves exhibit discontinuities near the value of e_C, approximately 0.41658. At this point, λ_q decreases discontinuously from higher to lower values as e_0 transitions through e_C from low to high values. The curves associated with smaller damping constants are generally higher than those with larger damping. Specifically, curve C_9 is greater than C_{10}, and C_{11} is greater than C_{12}. When $e_0 > e_C$, all curves exhibit small fluctuations around nearly horizontal lines, and C_{10} and C_{12} showing negative values.

The Lyapunov exponents, λ_q, versus amplitude, e_0, with the frequency fixed at $f = 5.0f_0$, are represented by curves C_{13} for $g = 0.01$ and C_{14} for $g = 0.3$, as shown in Figure 5. The amplitude, e_0, varies from $0.025e_C$ to $10.0e_C$. In Figure 5, both C_{13} and C_{14} exhibit a discontinuity near the value of e_C, approximately 0.41658. However, the discontinuity in C_{14} is less severe and exhibits a rounded structure as e_0 transitions through e_C from low to high values. The curves associated with smaller damping constants are generally higher than those with larger damping constants. Specifically, curve C_{13} is greater than C_{14}. When $e_0 > e_C$, curve C_{13} exhibits small fluctuations around nearly horizontal lines. In contrast, curve C_{14} exhibits larger fluctuations, including a few periodic windows corresponding to the parts of C_{14} located below the horizontal axis.

Order parameter responses in bulk AFE

The third part is based on the results obtained from the first two parts. A few sets of values for f and e_0 are chosen to generate the phase portraits of the AFE system using the fourth-order Runge-Kutta method, following the approach outlined in (Lim 2022). The selection of f and e_0 values is made with the aim of observing the relations between λ_q and the responses of the AFE to the applied electric field. For the purpose of comparison, two sets of numerical data are generated for each selected f and e_0 combination: one set corresponds to a small damping value of $g = 0.01$, and the other set corresponds to a large damping value of $g = 0.3$.

The calculated data for each set of f, e_0, and g values are plotted in four figures. (a) shows the plot of the dimensionless applied sinusoidal electric field, e, and the dimensionless normal displacement, q, as functions of dimensionless time, t. (b) shows hysteresis features, i. e., the dimensionless normal displacement, q, versus the dimensionless applied electric field, e. (c) shows the phase portrait of the system, namely, the time derivative of the dimensionless normal displacement, dq/dt, versus the dimensionless normal displacement, q. Lastly, (d) exhibits the states of the AFE system in the dimensionless phase space plotted against dimensionless time, t, in a three-dimensional curve. The duration for the numerical results shown in (a) to (d) is four cycles, specifically from the 31st to the 34th cycles.

For $e_0 = 1.0 \times 10^{-12}$ $e_C = 4.1658 \times 10^{-13}$ and $f = 4.0 \times 10^{-3}$ $f_0 \approx 8.5346 \times 10^{-5}$, the AFE responses are shown in Figure 6(a) to 6(d). The curves corresponding to the damping constant g, equalling 0.01 and 0.3, overlap with a difference of approximately 2% between the two sets of numerical data. The maximal

Lyapunov exponent for the g = 0.3 case is positive, approximately 3.58144. However, the computation of λ_q for the g = 0.01 case encounters numerical simulation overflow, preventing its generation. The responses of the AFE exhibit characteristics close to periodic responses. This can be observed in Figure 6(a), where the curves resemble sinusoidal curves and are in phase with e. Furthermore, the curves in the four cycles overlap, resulting in a linear line through the origin in Figure 6(b) and an elliptical shape in the phase portrait shown in Figure 6(c). For a particular set of e_0 and f values, the magnitude of the order parameter response is proportional to the area occupied by the corresponding phase portrait, or the volume V_q in (dq/dt, q) in phase space. The area occupied by the ellipse in Figure 6(c) is estimated as $V_q \approx 1.025 \times 10^{-29}$, which is extremely small due to the smallness of the applied e_0 and f values. The smooth curve in Figure 6(d) further elaborates the elliptical phase portrait shown in Figure 6(c).

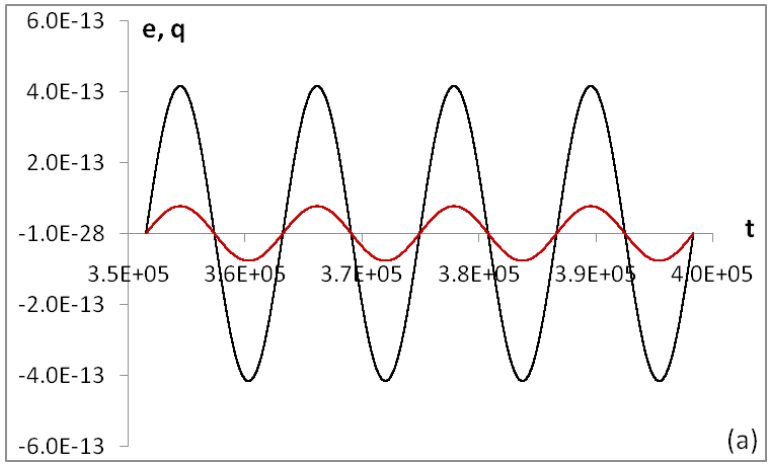

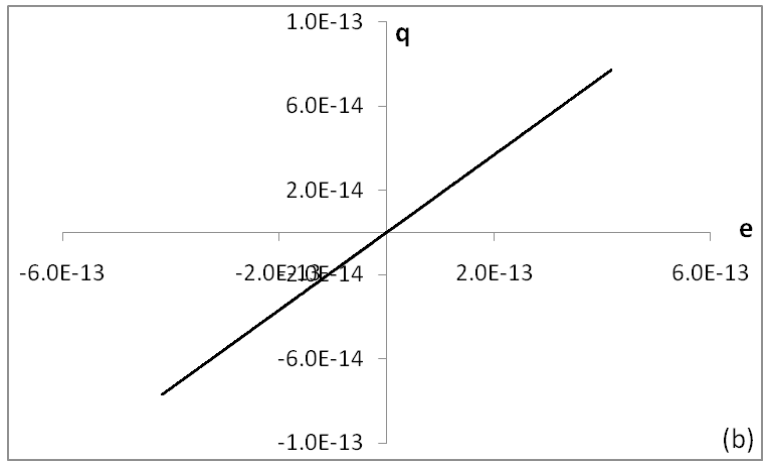

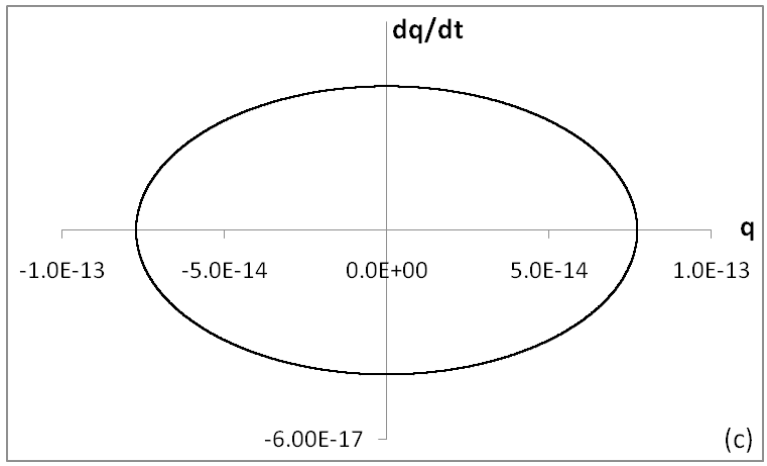

 https://www.doi.org/10.33910/2687-153X-2023-4-4-176-194

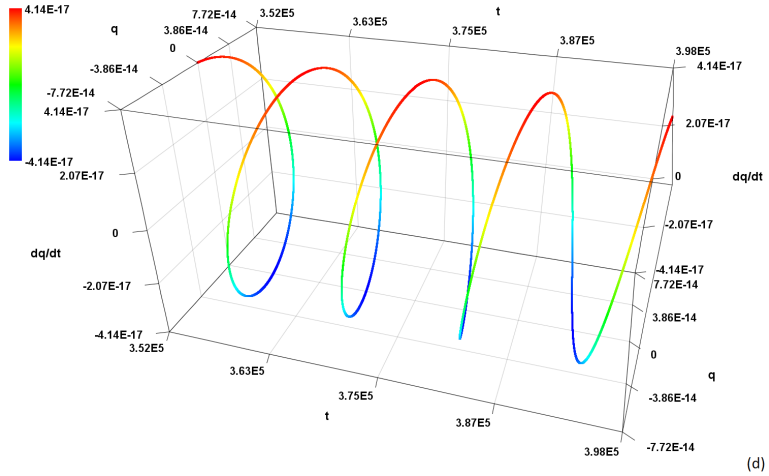

Fig. 6. AFE response for $f = 4.0 \times 10^{-3} f_0$, $e_0 = 1.0 \times 10^{-12} e_C$, $g = 0.3$ and 0.01. (a) e and q versus t, where e is represented by the black curve and q is represented by the red curve. (b) q versus e. (c) dq/dt versus q. (d) dq/dt versus q versus t.

For $e_0 = 0.9e_C \approx 0.374922$, $f = 2.275\, f_0 \approx 0.048541$, and $g = 0.3$, the AFE responses are shown in Figure 7(a) to 7(d). The maximal Lyapunov exponent is positive and approximately 3.477528. In Figure 7(a), the curves of e and q exhibit a slight phase difference. The q curve shows wavy deviation on triangular waves. The hysteresis loops and corresponding phase portraits for four cycles of e overlap, as depicted in Figures 7(b) and 7(c). Figure 7(c) shows that the AFE responses occupy a small volume in phase space, estimated at $V_q \approx 0.0105$. The wavy pattern observed in each cycle of the curve in Figure 7(d) further elaborates the non-elliptic irregular wavy cloud shape of the phase portrait shown in Figure 7(c).

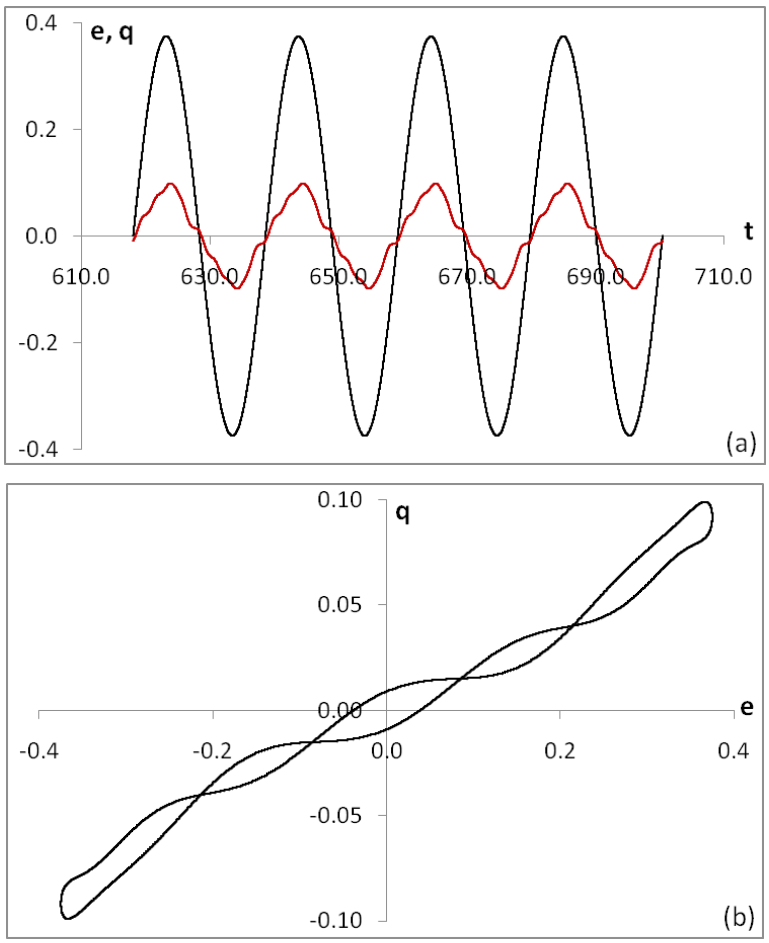

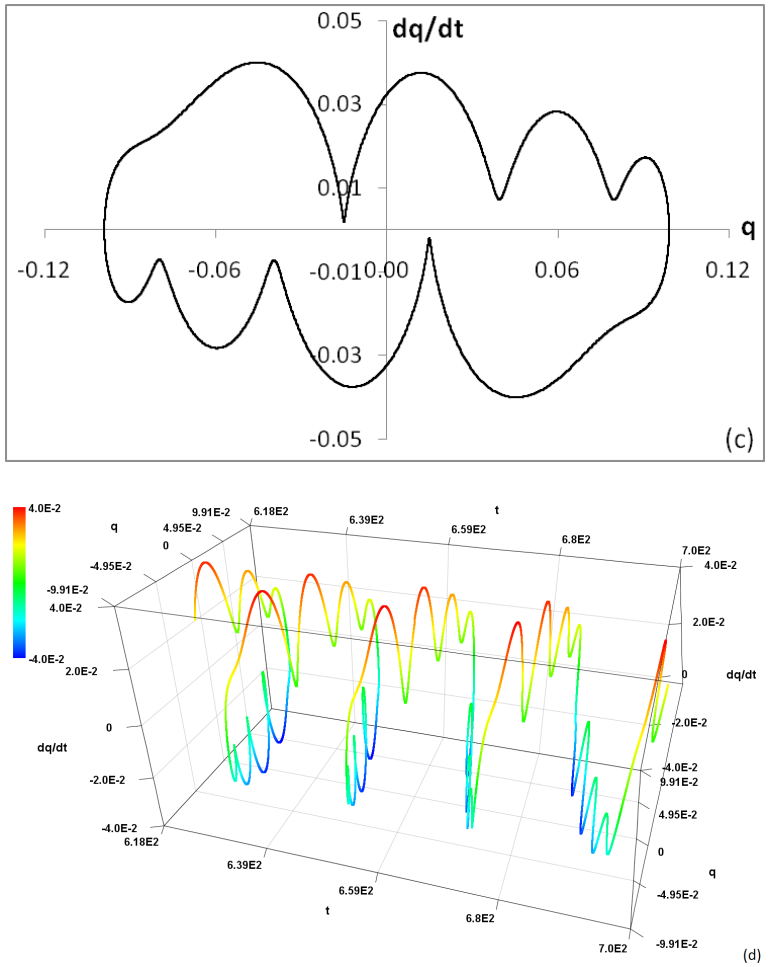

Fig. 7. AFE response for $f = 2.275f_0$, $e_0 = 0.9e_C$, $g = 0.3$. $\lambda_q = 3.4775278$. (a) e and q versus t, where e is represented by the black curve and q is represented by the red curve. (b) q versus e. (c) dq/dt versus q. (d) dq/dt versus q versus t.

For $e_0 = 0.9e_C \approx 0.374922$, $f = 2.275f_0 \approx 0.048541$, and $g = 0.01$, the AFE responses are shown in Figure 8(a) to 8(d). The maximal Lyapunov exponent is positive and approximately 1.185748. In Figure 8(a), e and q exhibit a slight phase difference. The pattern of the q curve shows an irregular wavy pattern on each cycle, indicating non-periodic behaviour. The hysteresis loops and corresponding phase portraits for four cycles of e do not overlap, as shown in Figures 8(b) and 8(c). Figure 8(c) shows that the responses of AFE occupy a volume $V_q \approx 2.44$ in phase space, which is about 232 times larger compared to the volume in Figure 7(c). The presence of additional irregular loops winding around the attractors on both sides in each cycle depicted in Figure 8(d) further elaborates the irregular and non-overlap dumbbell shapes of the phase portrait displayed in Figure 8(c).

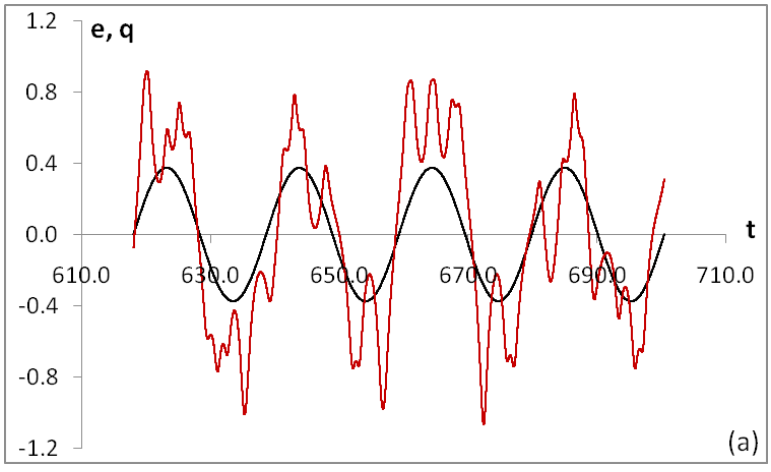

 https://www.doi.org/10.33910/2687-153X-2023-4-4-176-194

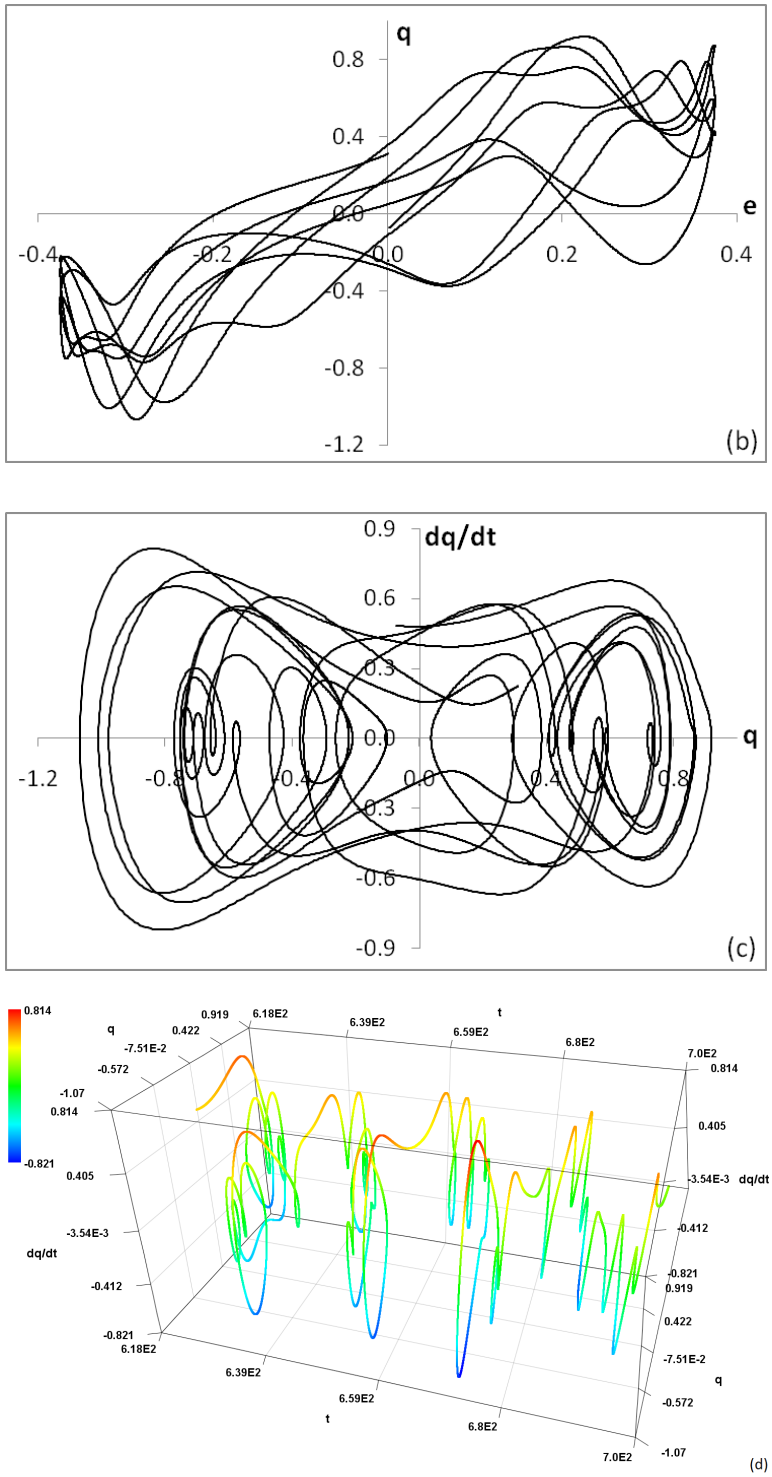

Fig. 8. AFE response for $f = 2.275 f_0$, $e_0 = 0.9 e_C$, $g = 0.01$, and $\lambda_q = 1.185748$. (a) e and q versus t, where e is represented by the black curve and q is represented by the red curve. (b) q versus e. (c) dq/dt versus q. (d) dq/dt versus q versus t.

For $e_0 = 0.9 e_C \approx 0.374922$, $f = 7.05\, f_0 \approx 0.150422$, and $g = 0.3$, the AFE responses are shown in Figure 9(a) to 9(d). The maximal Lyapunov exponent is positive and approximately 0.380776. In Figure 9(a), e and q are out of phase, with q leading e nearly $\pi/4$. The pattern of the q curve exhibits slightly distorted triangular waves. The hysteresis loops and corresponding portraits for four cycles of e overlap, as shown in Figures 9(b) and 9(c). Figure 9(c) demonstrates that the responses of the AFE occupy a volume $V_q \approx 3.22$ in phase space. The pattern observed in each cycle of the curve in Figure 9(d) further elaborates the dumbbell shape of the phase portrait displayed in Figure 9(c).

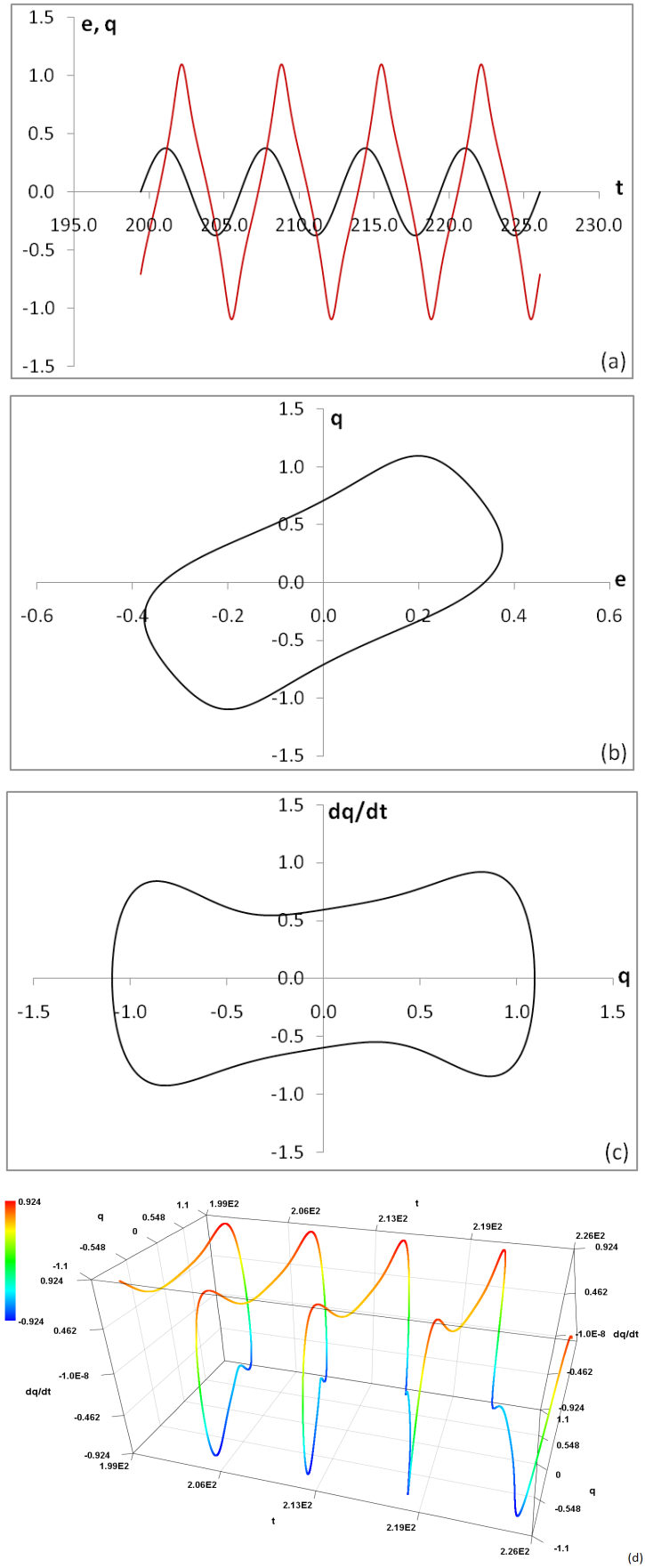

Fig. 9. AFE response for $f = 7.05f_0$, $e_0 = 0.9e_C$, $g = 0.3$, and $\lambda_q = 0.3807764$. (a) e and q versus t, where e is represented by the black curve and q is represented by the red curve. (b) q versus e. (c) dq/dt versus q. (d) dq/dt versus q versus t.

 https://www.doi.org/10.33910/2687-153X-2023-4-4-176-194

For $e_0 = 0.9e_C \approx 0.374922$, $f = 7.05f_0 \approx 0.150422$, and $g = 0.01$, the AFE responses are shown in Figure 10(a) to 10(d). The maximal Lyapunov exponent is positive and approximately 0.826725. In Figure 10(a), e and q are out of phase. The pattern of the q curve shows an irregular wavy pattern on each cycle, indicating non-periodic behaviour. The hysteresis loops and corresponding phase portraits for four cycles of e do not overlap as shown in Figures 10(b) and 10(c). Figure 10(c) shows that the responses of AFE occupy a volume $V_q \approx 2.92$ in phase space, which is slightly smaller than the one shown in Figure 9(c). The irregular wavy curve in Figure 10(d) further elaborates the irregular shape of the phase portrait displayed in Figure 10(c).

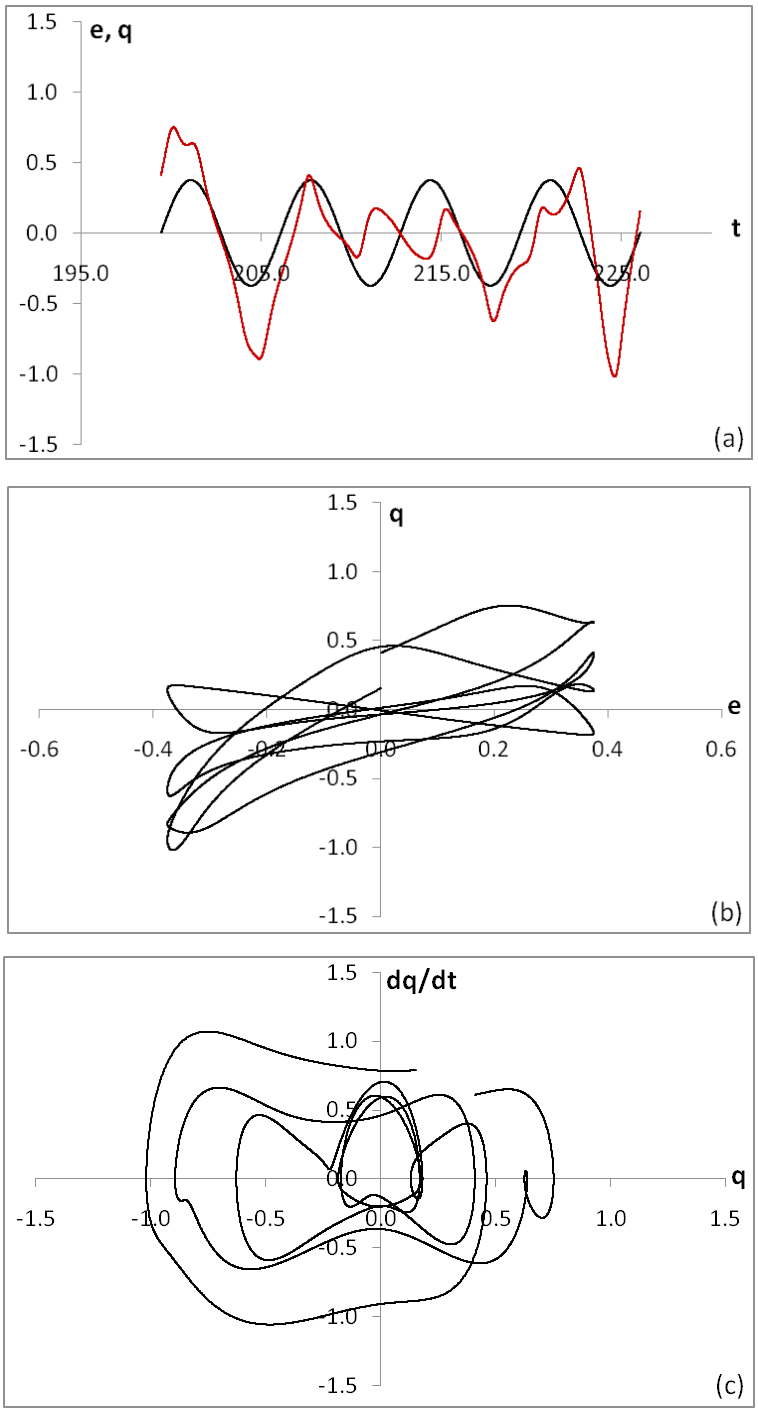

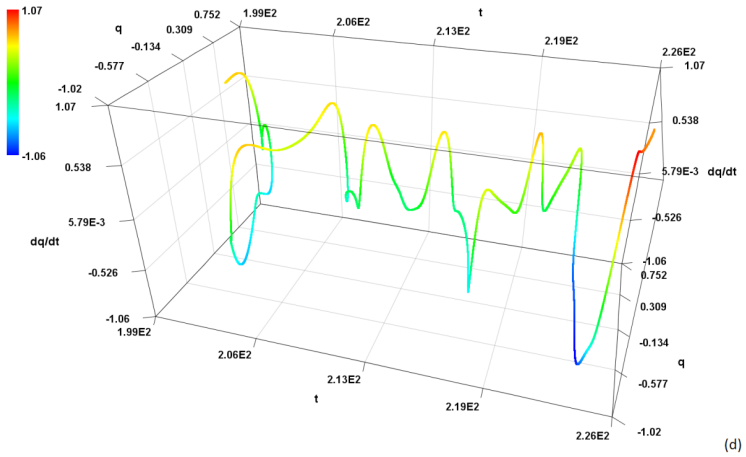

Fig. 10. AFE response for $f = 7.05f_0$, $e_0 = 0.9e_C$, $g = 0.01$, and $\lambda_q = 0.82672474$. (a) e and q versus t, where e is represented by the black curve and q is represented by the red curve. (b) q versus e. (c) dq/dt versus q. (d) dq/dt versus q versus t.

For $e_0 = 2.0e_C \approx 0.83316$, $f = 0.025\, f_0 \approx 5.334131 \times 10^{-4}$, and $g = 0.3$, the AFE responses are shown in Figures 11(a) to 11(d). The maximal Lyapunov exponent is negative and approximately –0.207926. In Figure 11(a), e and q are out of phase. The q wave exhibits branching spikes on the first and third quadrant edges of every cycle, indicating periodic behaviour. The hysteresis loops and corresponding phase portraits for four cycles of e overlap, as shown in Figures 11(b) and 11(c). Figure 11(c) exhibits inward spiral curves towards the attractors located at both sides, corresponding to $q \approx \pm 0.89$. The responses of the AFE occupy a volume $V_q \approx 2.71$ in phase space. The anti-symmetric dumbbell-shaped 4-cycle curve spiraling towards the attractors on both sides for each cycle depicted in Figure 11(d) further elaborates on the pattern observed in the phase portrait displayed in Figure 11(c).

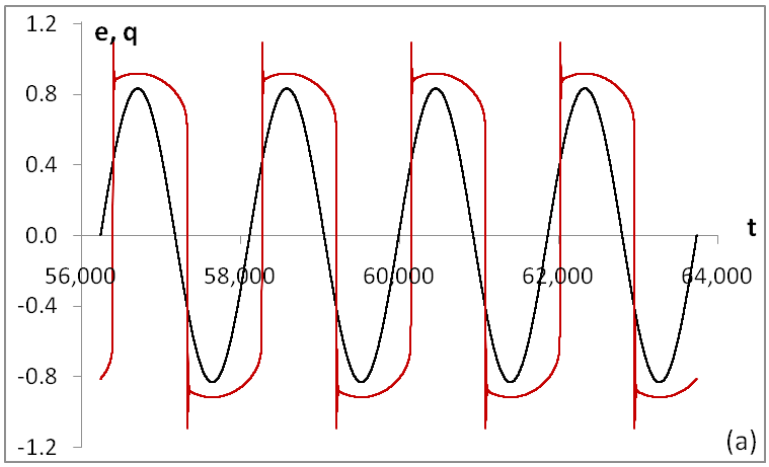

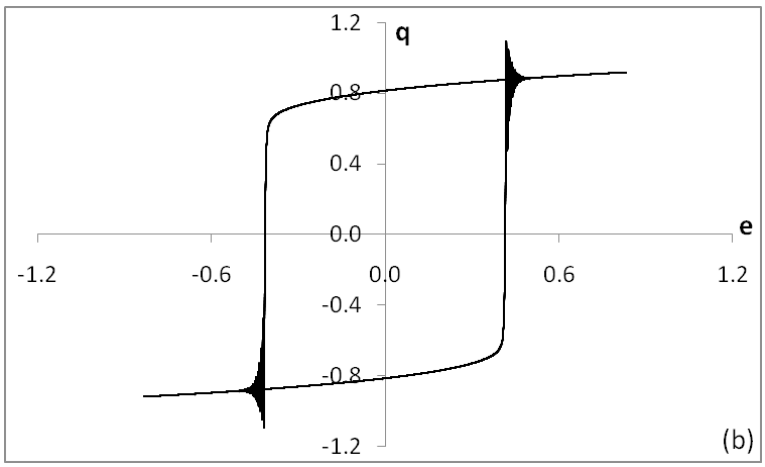

https://www.doi.org/10.33910/2687-153X-2023-4-4-176-194

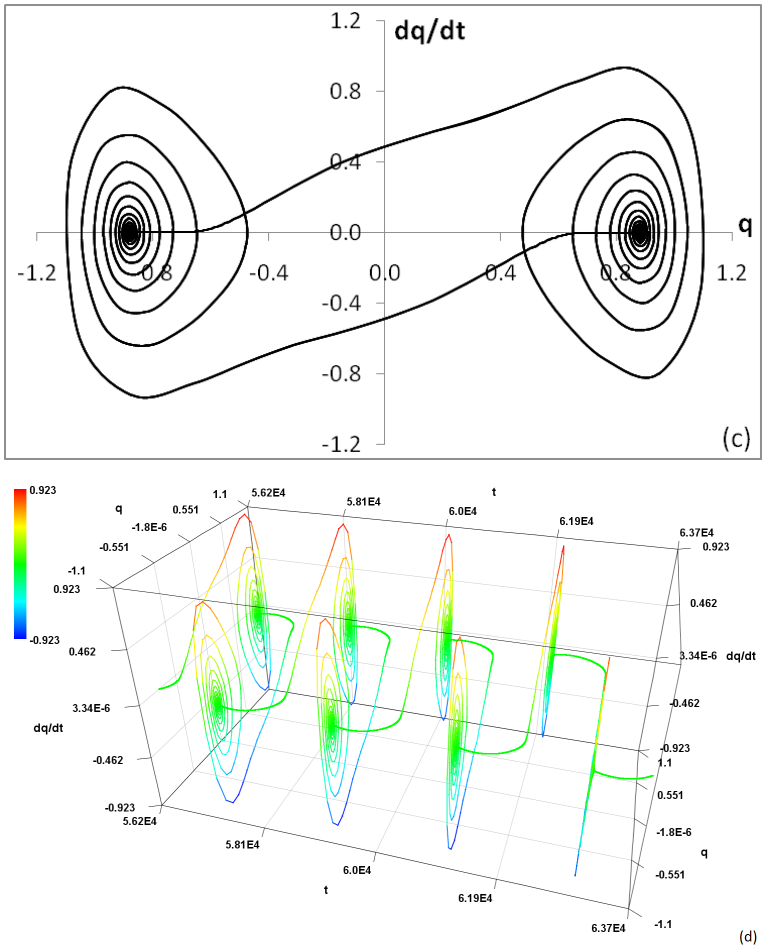

Fig. 11. AFE response for $f = 0.025 f_0$, $e_0 = 2.0e_C$, $g = 0.3$, and $\lambda_q = -0.20792619$. (a) e and q versus t, where e is represented by the black curve and q is represented by the red curve. (b) q versus e. (c) dq/dt versus q. (d) dq/dt versus q versus t.

For $e_0 = 2.0e_C \approx 0.83316$, $f = 0.025 f_0 \approx 5.334131 \times 10^{-4}$, and $g = 0.01$, the AFE responses are shown in Figure 12(a) to 12(d). The maximal Lyapunov exponent is negative and approximately −0.00414195. In Figure 12(a), e and q are out of phase. The q wave exhibits intense branching oscillations damped towards the peaks of the first and third quadrant of every cycle, indicating periodic behaviour. The hysteresis loops and corresponding phase portraits for four cycles of e overlap, as shown in Figures 12(b) and 12(c). Figure 12(c) illustrates intense inward spiral curves towards the attractors located at both sides, corresponding to $q \approx \pm 0.89$, The responses of the AFE occupy a volume $V_q \approx 4.12$ in phase space, which is approximately 1.52 times larger than the one shown in Figure 11(c). The anti-symmetric dumbbell-shape 4-cycles curve, spiraling towards the attractors on both sides for each cycle in Figure 12(d), further elaborates on the pattern observed in the phase portrait displayed in Figure 12(c).

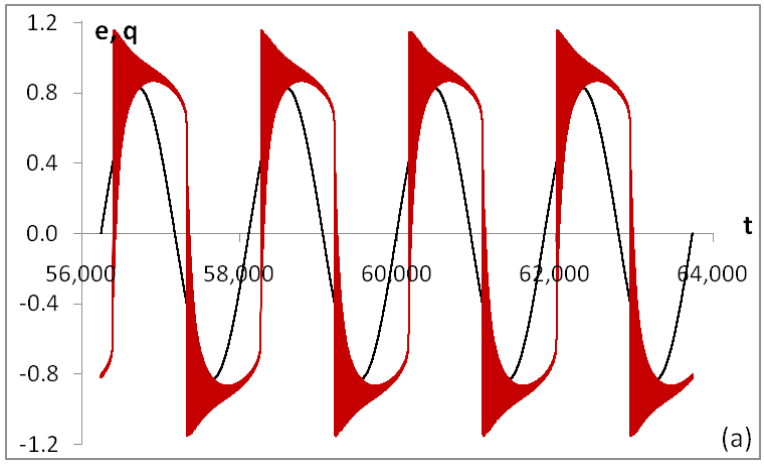

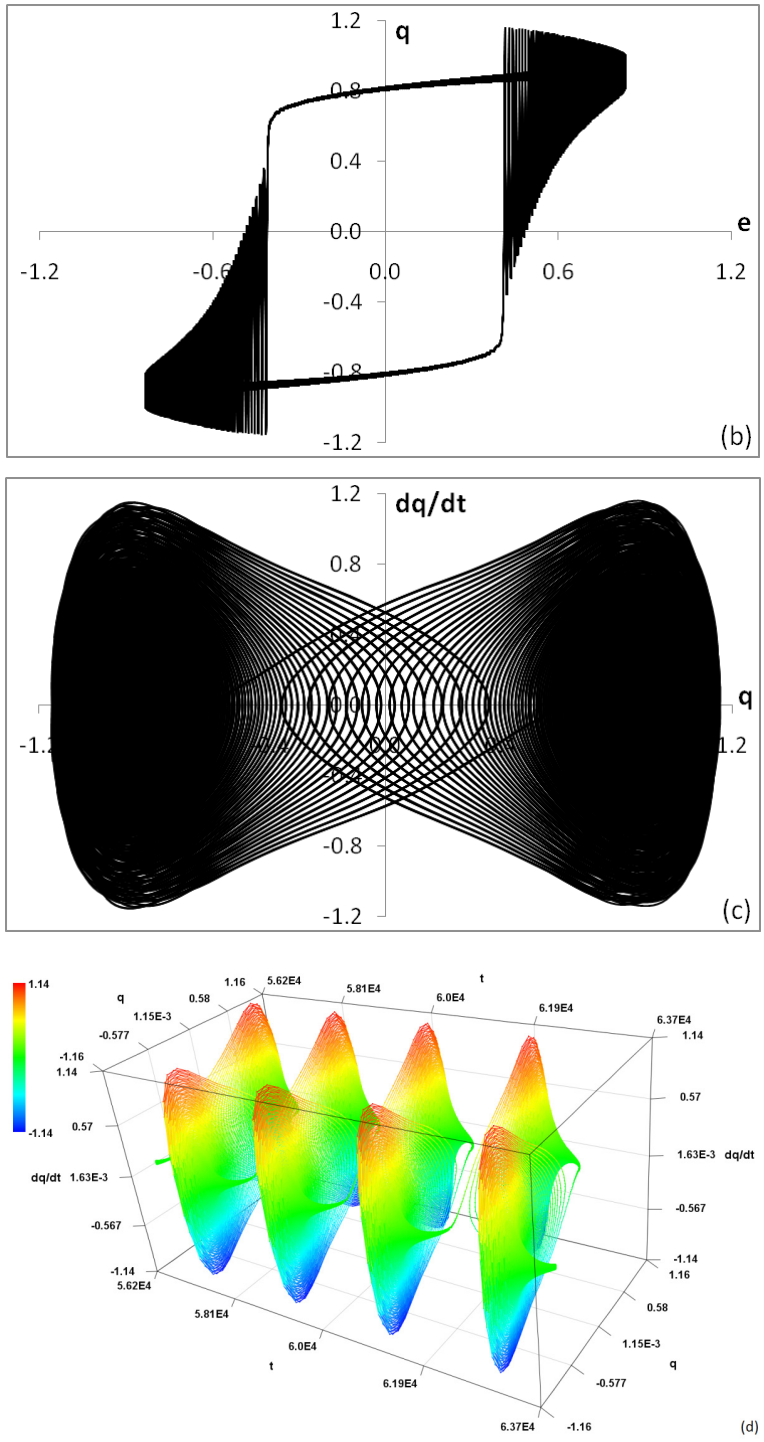

Fig. 12. AFE response for $f = 0.025\,f_0$, $e_0 = 2.0e_C$, $g = 0.01$, and $\lambda_q = -0.0041419531$. (a) e and q versus t, where e is represented by the black curve and q is represented by the red curve. (b) q versus e. (c) dq/dt versus q. (d) dq/dt versus q versus t.

For $e_0 = 249.0e_C \approx 103.7284$, $f = 25.5\,f_0 \approx 0.544081$, and $g = 0.3$, the AFE responses are shown in Figures 13(a) to 13(d). The maximal Lyapunov exponent is negative, approximately −0.218945. In Figure 13(a), e and q are slightly out of phase. The pattern of the q curve exhibits slightly distorted triangular waves with two branching peaks and troughs. It is periodic, as indicated by the overlap of the hysteresis loops and corresponding phase portraits for four cycles of e shown in Figures 13(b) and 13(c). Figure 13(c) shows that the responses of the AFE occupy a volume $V_q \approx 95.54$ in phase space. In Figure 13(d), the curve exhibits two windings around each attractor in each cycle, further elaborating on the dumbbell-shaped loops with extra windings on both sides of the phase portrait shown in Figure 13(c).

 https://www.doi.org/10.33910/2687-153X-2023-4-4-176-194

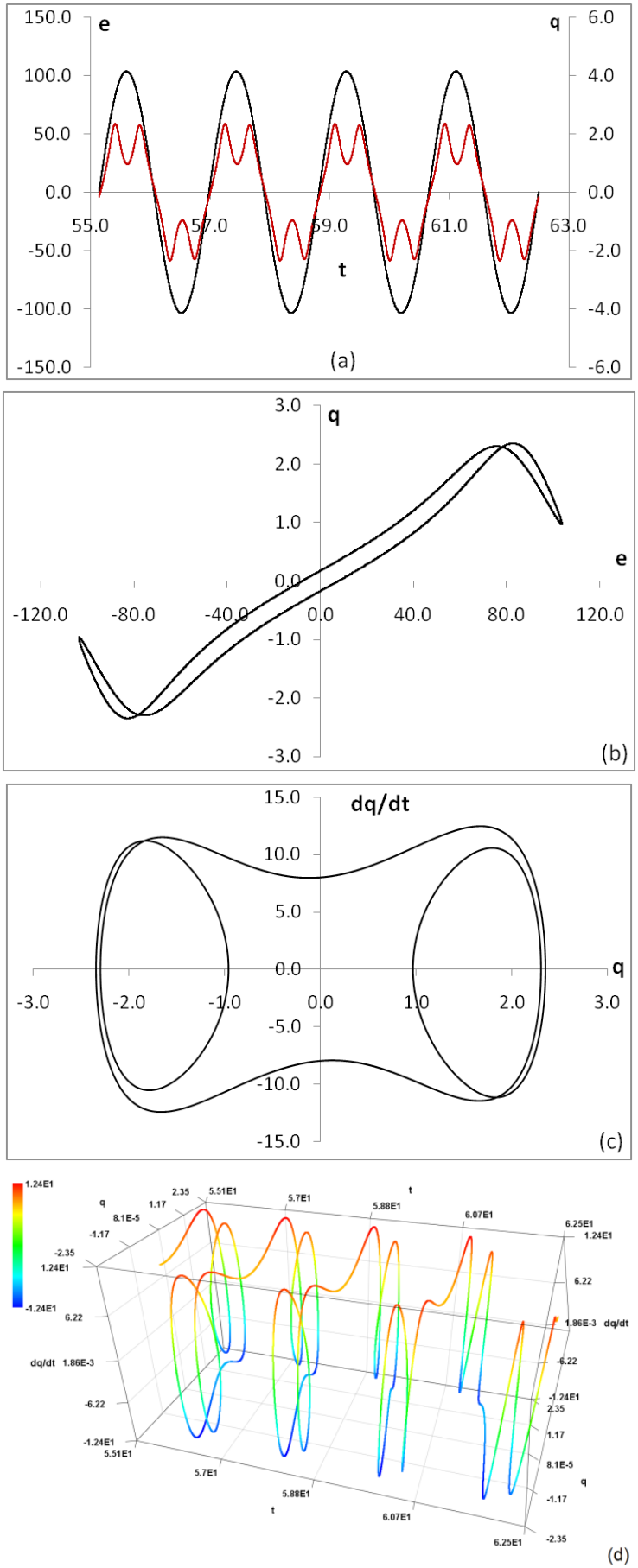

Fig. 13. AFE response for $f = 25.5f_0$, $e_0 = 249e_C$, $g = 0.3$, and $\lambda_q = -0.218945$. (a) e and q versus t, where e is represented by the black curve and q is represented by the red curve. (b) q versus e. (c) dq/dt versus q. (d) dq/dt versus q versus t.

For $e_0 = 249.0 e_C \approx 103.7284$, $f = 25.5 f_0 \approx 0.544081$, and $g = 0.01$, the AFE responses are shown in Figures 14(a) to 14(d). The maximal Lyapunov exponent is positive, approximately 3.230842. Figures 14(a) to 14(d) exhibit similar characteristics to Figures 8(a) to 8(d) and Figures 10(a) to 10(d), with the exception that the responses of the AFE occupied a large volume, $V_q \approx 197.24$, in phase space, which is approximately double compared to the one shown in Figure 13(c).

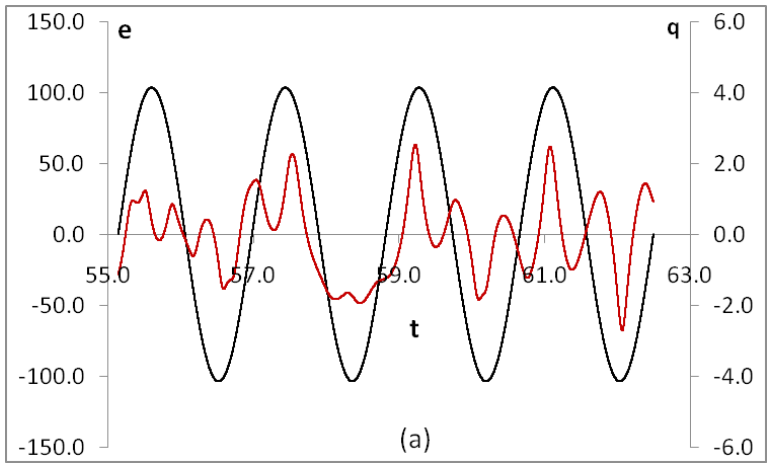

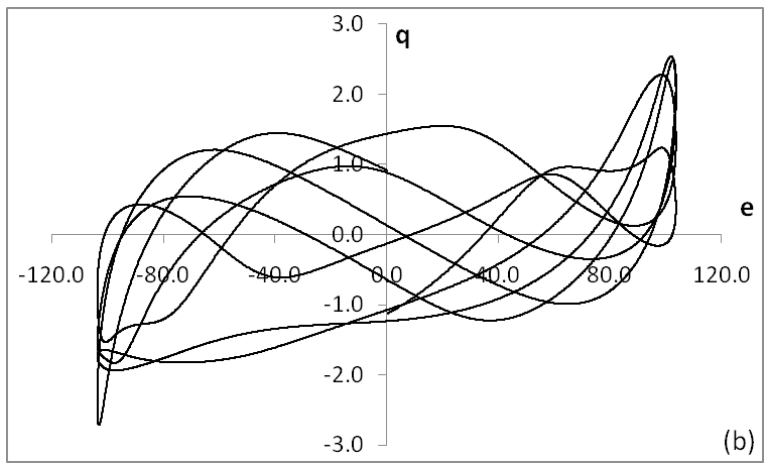

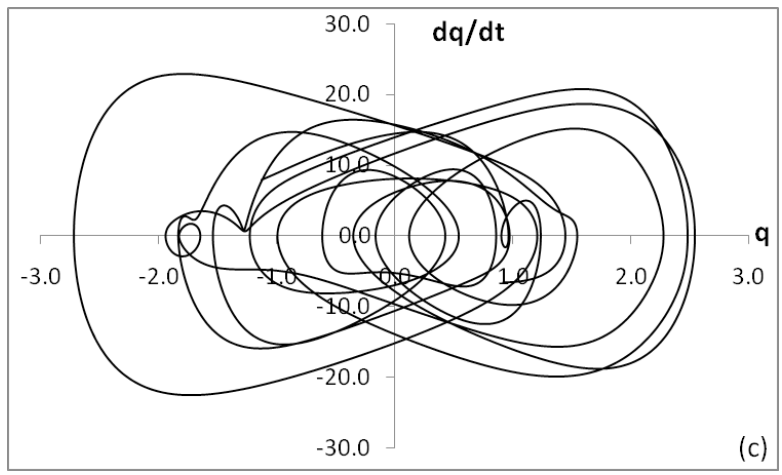

 https://www.doi.org/10.33910/2687-153X-2023-4-4-176-194

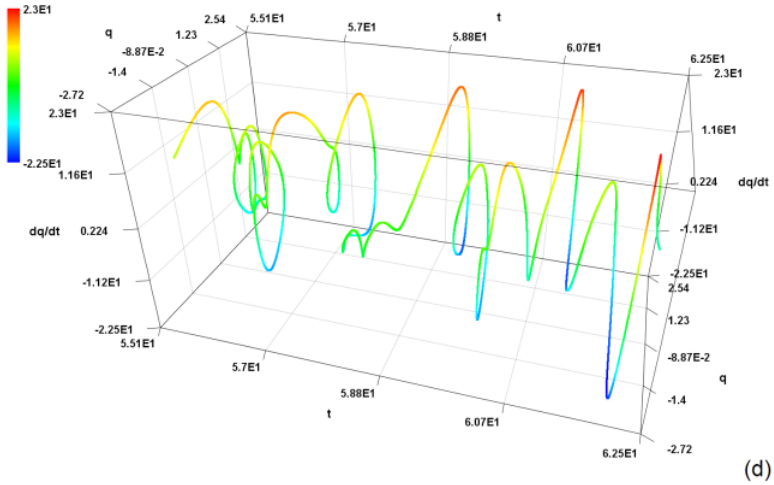

Fig. 14. AFE response for $f = 25.5f_0$, $e_0 = 249e_C$, $g = 0.01$, and $\lambda_q = 3.230842$. (a) e and q versus t, where e is represented by the black curve and q is represented by the red curve. (b) q versus e. (c) dq/dt versus q. (d) dq/dt versus q versus t.

Conclusions

The results of the first part indicate that, for small amplitudes (e_0) and frequencies (f) of the applied field, the Lyapunov exponents (λ_q) for $g = 0.01$ are greater than those for $g = 0.3$. Additionally, most of the periodic windows, corresponding to $\lambda_q < 0$, are observed in curves with a large damping constant ($g = 0.3$).

In the second part, it is observed that as the amplitude of the applied field (e_0) varies from low values and sweeps through e_C to high values, the Lyapunov exponents (λ_q) decrease discontinuously at $e_0 \approx e_C$, regardless of the frequency. Furthermore, for applied fields with low frequencies ($f \le 0.5f_0$) and amplitudes greater than the cohesive field ($e_0 > e_C$), in a system with large damping ($g = 0.3$), the Lyapunov exponents (λ_q) are negative.

The results from the third part demonstrate that the time-varying dimensionless normal displacements (q) are distorted compared to the sinusoidal applied field (e). It is observed that, for the negative Lyapunov exponents, the trajectories in phase space spiral towards attractors regardless of damping. The magnitude of the system's responses is proportional to the volume in phase space (V_q) occupied by the trajectories.

In most cases, V_q is smaller for large damping and larger for small damping, as shown in Figures 6(c) to 8(c) and 11(c) to 14(c). For cases near e_C, the relative responses exhibit large fluctuations with respect to frequency. For example, when $e_0 = 0.9e_C$ and $f = 2.275f_0$, V_q for large damping ($g = 0.3$) in Figure 7(c) is approximately 232 times smaller than V_q for small damping ($g = 0.01$) in Figure 8(c). Conversely, when $e_0 = 0.9e_C$ and $f = 7.05f_0$, V_q for large damping in Figure 9(c) is approximately 1.1 times larger than V_q for small damping in Figure 10(c). In general, large damping tends to suppress chaos when e_0 is not close to e_C.

For cases with large damping and positive λ_q, the orbits of trajectories exhibit significant overlap across consecutive cycles of the driving field, as shown in Figures 6(c), 7(c), and 9(c). When λ_q is negative, the responses are periodic, and the orbits of trajectories spiral towards attractors, particularly for moderate values of amplitude values (e. g., $e_0 = 2.0e_C$) and low frequencies (e. g., $f = 0.025f_0$). However, this effect is less obvious for large value of amplitude values (e. g., $e_0 = 249.0e_C$) and high frequencies (e. g., $f = 25.5f_0$).

As a summary, the numerical results demonstrate that periodic responses occur when $\lambda_q < 0$, as shown in Figures 11 to 13. When e_0 and f are very small, irrespective of the damping, λ_q is positive, leading to quasi-periodic responses. For moderate values of e_0 and f, when $\lambda_q > 0$, the responses with damping $g = 0.01$ exhibit chaotic behaviour, as shown in Figures 8, 10, and 14, while the responses with damping $g = 0.3$ appear quasi-periodic, as indicated by the overlapping hysteresis loops and phase portraits in Figures 7 and 9. Larger damping in the AFE system reduces the chaotic response and the density of chaos. Consequently, large damping can regulate response to the driving field, even though the system is chaotic.

Based on the comprehensive numerical results, we conclude that, for the antiferroelectric system in its first-order phase, the method of calculating the Lyapunov exponent and plotting phase portraits proves to be an efficient approach for identifying the regimes of amplitude and frequency of the applied field that lead to periodic and chaotic responses, particularly in the case of small damping. This approach offers an alternative to studying chaotic dynamics through multiple phase portraits (Lim 2022). The numerical simulations confirm that by manipulating the amplitude, frequency, and damping parameters of the AFE system, it is possible to control and regulate the occurrence of chaotic and periodic responses in the bulk AFE system. Utilizing the largest Lyapunov exponent as an informative indicator for characterizing the system's nonlinear behaviors proves to be an effective approach.

Conflict of Interest

The author declares that there is no conflict of interest, either existing or potential.

References

Baker, G. L., Gollub, J. P. (1996) *Chaotic dynamics: An introduction*. 2nd ed. Cambridge: Cambridge University Press, 268 p. (In English)

Benettin, G., Pasquali, S., Ponno, A. (2018) The Fermi-Pasta-Ulam problem and its underlying integrable dynamics: An approach through Lyapunov Exponents. *Journal of Statistical Physics*, 171 (4), 521–542. https://doi.org/10.1007/s10955-018-2017-x (In English)

Boyce, W. E., DiPrima, R. C. (2001) *Elementary differential equations and boundary values problems*. 7th ed. Singapore: John Wiley & Sons Publ., 745 p. (In English)

Dykman, M. I., Mannella, R., McClintock, P. V. E. et al. (1988) Spectral density of fluctuation of a double-well Duffing oscillator driven by white noise. *Physical Review A*, 37 (4), 1303–1312. https://doi.org/10.1103/PhysRevA.37.1303 (In English)

Goldstein, H., Poole, C., Safko, J. (2002) *Classical mechanics*. 3rd ed. Boston: Addison–Wesley Publ., 665 p. (In English)

Lega, E., Guzzo, M., Froeschlé, C. (2016) Theory and applications of the fast Lyapunov indicator (FLI) method. In: C. Skokos, G. Gottwald, J. Laskar (eds.). *Chaos Detection and Predictability*. Berlin; Heidelberg: Springer Publ., pp. 35–54. http://dx.doi.org/10.1007/978-3-662-48410-4_2 (In English)

Lim, S.-Ch. (2022) Numerical simulations of nonlinear and chaotic order parameter responses in bulk antiferroelectrics using ammonium dihydrogen phosphate parameter. *Physics of Complex Systems*, 3 (3), 122–136. https://www.doi.org/10.33910/2687-153X-2022-3-3-122-136 (In English)

Marion, J. B., Thornton, S. T. (1995) *Classical dynamics of particles and systems*. 4th ed. New York: Harcourt College Publ., 672 p. (In English)

Meunier, T., LaCasce, J. H. (2021) The finite size lyapunov exponent and the finite amplitude growth rate. *Fluids*, 6 (10), article 348. https://doi.org/10.3390/fluids6100348 (In English)

Strogatz, S. H. (2015) *Nonlinear dynamics and chaos with applications to Physics, Biology, Chemistry, and Engineering*. 2nd ed. New York: CRC Press, 532 p. https://doi.org/10.1201/9780429492563 (In English)

Wolf, A., Swift, J. B., Swinney, H. L., Vastano, J. A. (1985) Determining lyapunov exponents from a time series. *Physica D: Nonlinear Phenomena*, 16 (3), 285–317. https://doi.org/10.1016/0167-2789(85)90011-9 (In English)